

# Silicon Composite Electrodes with Dynamic Ionic Bonding

Sen Kang, Ke Yang, Scott R. White, and Nancy R. Sottos\*

**Silicon (Si) composite electrodes are developed with increased cycle lifetimes and reliability through dynamic ionic bonding between active Si nanoparticles and a polymer binder. Amine groups are covalently attached to Si nanoparticles via surface functionalization. Si composite electrodes are fabricated by combining the Si nanoparticles with a poly(acrylic acid) (PAA) binder. The formation of ionic bonds between amine groups on Si particles and carboxylic acid groups on the PAA binder is characterized by X-ray photoelectron spectroscopy and Raman spectroscopy. Si composite anodes with ionic bonding demonstrate long term cycling stability with capacity retention of 80% at 400 cycles at a current density of 2.1 A g<sup>-1</sup> and good rate capability. The dynamic ionic bonds effectively mitigate the deterioration of electrical interfaces in the composite anodes as suggested by stable impedance over 300 cycles.**

## 1. Introduction

Lithium-ion batteries are widely used in portable electronic devices, electric vehicles, and grid-scale energy storage due to the high energy density, high power density, and high operating voltages.<sup>[1,2]</sup> Graphite is the active material for most commercial anodes and has a capacity of 372 mAh g<sup>-1</sup>. The growing need for anode materials with higher capacity has led to the investigation of silicon due to its high gravimetric capacity (4200 mAh g<sup>-1</sup>) and volumetric capacity (9786 mAh cm<sup>-3</sup>).<sup>[3]</sup> However, Si undergoes large volume change (>400%) upon lithiation, resulting in fracture of Si, loss of conductivity, an unstable solid electrolyte interface (SEI) layer on the Si particle surface, and rapid capacity decrease.<sup>[4]</sup> Significant research efforts have been devoted to address these challenges.<sup>[5,6]</sup> Specific materials strategies to overcome these degradation mechanisms brought about due to the large volume change of Si include the use of Si particles dispersed in a rigid carbon matrix, Si thin films, nanostructured Si, and nanoparticle Si composite anodes with polymer binders.<sup>[7–10]</sup> In this paper, we explore the use of dynamic ionic interfacial bonding in

nanoparticle Si composite electrodes to achieve stable, high capacity performance.

Polyvinylidene fluoride (PVDF) is one of the most common binders in graphite composite electrodes, but has only weak van der Waals interactions with Si particles.<sup>[11]</sup> In contrast, polymer binders containing carboxyl groups, such as carboxyl-methyl cellulose (CMC), poly(acrylic acid) (PAA), and alginate, form strong hydrogen bonds with the native silica layer on Si particle surfaces, resulting in much better capacity retention of the Si anodes.<sup>[12–14]</sup> Bridel et al. suggested that the hydrogen bonds undergo a self-healing process that is crucial for cycling stability of Si anodes.<sup>[15]</sup> Furthermore, a self-healing

hydrogen bonding polymer binder has been incorporated in a composite electrode containing Si microparticles.<sup>[16,17]</sup> The self-healing composite anodes demonstrated 80% capacity retention after 175 cycles at a current density of 0.42 A g<sup>-1</sup>. More recently, Sun et al., developed a high-capacity stretchable graphitic carbon/Si foam electrode that was enabled by a conformal self-healing elastic polymer coating.<sup>[18]</sup>

Other types of dynamic bonds such as metal–ligand coordination bonds,  $\pi$ – $\pi$  stacking, and ionic bonds can impart self-healing properties to polymers.<sup>[19]</sup> Ionic bonding involves two oppositely charged ions and is generally stronger than hydrogen bonding. Battery electrolyte consists of aprotic polar solvents (typically organic carbonates) and dissolved lithium salt, which facilitates the dynamic nature of the ionic bonding in the composite electrode.<sup>[20]</sup> Sun et al.<sup>[21]</sup> developed a stretchable and tough hydrogel by mixing both a covalently cross-linked polyacrylamide matrix with an ionically cross-linked alginate network. The carboxylate/Ca<sup>2+</sup> ionic bond in the alginate network was broken upon stretching the hydrogel and then reformed upon unloading to effectively heal internal damage. Similarly, Wei et al.<sup>[22]</sup> prepared self-healing hydrogels consisting of ferric ions and ionically cross-linked PAA. The migration of Fe<sup>3+</sup> in the hydrogel allowed for reformation of carboxylate/Fe<sup>3+</sup> ionic bonds after damage. In addition, a self-healing anticorrosion coating was developed by Andreeva et al.<sup>[23]</sup> via layer-by-layer deposition of polyelectrolytes on an Al substrate consisting of poly(ethyleneimine) as polycation and poly(styrene sulfonate) as polyanion. Finally, South and Lyon<sup>[24]</sup> described a self-healing hydrogel film fabricated by layer-by-layer assembly of an anionic microgel and cationic amine. After the damage, solvation of the film in water permitted the reformation of the ionic bonds and recovery for multiple cycles of damage and healing.

Combining the positive role that dynamic bonds play in improving Si anode's performance and ionic interaction plays in self-healing materials, here we report a simple yet versatile approach to incorporate dynamic ionic bonds in Si composite

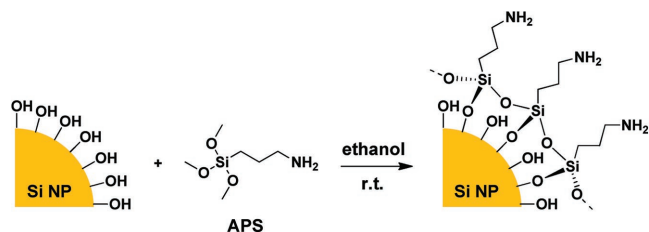
Dr. S. Kang, Dr. K. Yang, Prof. S. R. White, Prof. N. R. Sottos  
Beckman Institute for Advanced Science and Technology  
University of Illinois at Urbana–Champaign  
61801 IL, USA

E-mail: n-sottos@illinois.edu

Dr. S. Kang, Dr. K. Yang, Prof. N. R. Sottos  
Materials Science and Engineering  
University of Illinois Urbana-Champaign  
Champaign, 61801 IL, USA

Prof. S. R. White  
Department of Aerospace Engineering  
University of Illinois at Urbana–Champaign  
61801 IL, USA

DOI: 10.1002/aenm.201700045



**Scheme 1.** Synthetic route for amine functionalized Si particles. APS was first hydrolyzed to produce silanol (Si–OH) groups, and then silanol groups condense with the hydroxyl groups on Si particles to form covalent Si–O–Si bonds by releasing H<sub>2</sub>O molecules.

anodes for autonomous healing of the anode during electrochemical operation. Ionic bonds were incorporated in Si anodes by surface functionalization of Si nanoparticles and using a poly(acrylic acid) binder. The formation of ionic bonds was confirmed by X-ray photoelectron spectroscopy and Raman spectroscopy. Si composite anodes with ionic bonding were characterized over 400 cycles and a variety of charge/discharge rate.

## 2. Results and Discussion

### 2.1. Surface Functionalization of Si Nanoparticles

Functionalization of Si materials with amine groups has been widely reported.<sup>[25,26]</sup> Si nanoparticles (denoted as Si NP) possess a thin native SiO<sub>2</sub> layer, which contains hydroxyl groups that can react with (3-aminopropyl)trimethoxysilane (APS) to covalently bond amine groups onto the Si particle surface (**Scheme 1**). Different amounts of APS were added to the functionalization solution to systematically vary the amine coverage on Si particles. The resulting surface amine coverage is summarized in **Figure 1** for five different APS/Si weight ratios. Increasing the amount of APS from 1:100 to 1:10 of APS/Si ratio (by mass) tripled the amine coverage from 0.0167 mmol g<sup>-1</sup> Si to 0.0512 mmol g<sup>-1</sup> Si. Further increase in the APS/Si ratio had no effect on the surface coverage. We hypothesized

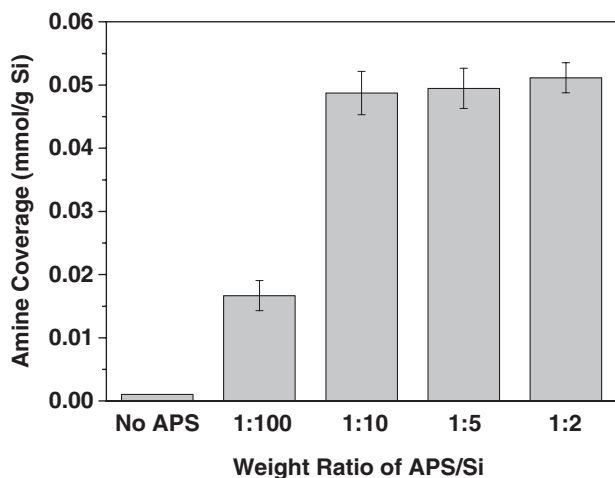
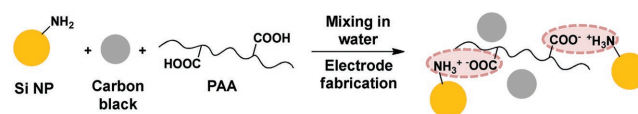


**Figure 1.** Effect of increasing the APS/Si weight ratio in the functionalization bath on the amine coverage of Si–NH<sub>2</sub> nanoparticles.



**Scheme 2.** Formation of interfacial ionic bonds between Si nanoparticles and PAA binder in Si composite anodes. The yellow spheres, grey spheres, and polymer chains represent Si–NH<sub>2</sub>, carbon black, and PAA binder, respectively.

that at 1:10 APS/Si weight ratio, the Si surface was saturated with amine groups due to steric effects which limited further reaction of APS on the Si particle.

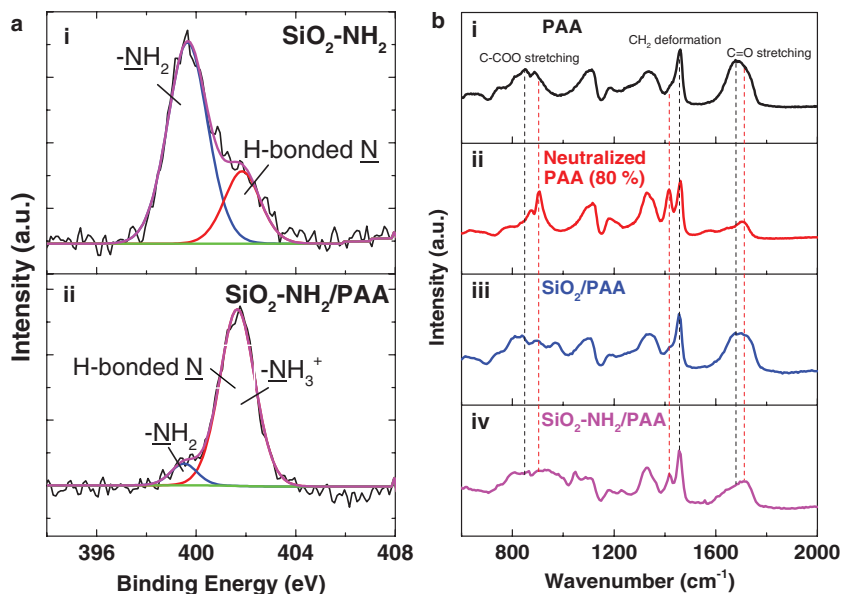
The amine functionalized Si (denoted as Si–NH<sub>2</sub>), conductive filler particles (carbon black), and PAA were mixed in water and dried to form the electrode. During mixing, amines from the Si–NH<sub>2</sub> deprotonate the carboxylic acids from the PAA polymer and form ionic ammonium carboxylate salt at the Si particle/PAA polymer binder interface (**Scheme 2**). The formation of ionic bonds was confirmed by X-ray photoelectron spectroscopy (XPS) and Raman spectroscopy using amino functionalized silica (denoted as SiO<sub>2</sub>–NH<sub>2</sub>). Due to strong absorption by the Si particles, Raman spectroscopy was noisy and a distinct PAA signal was not discernable. Instead, identically functionalized silica particles (SiO<sub>2</sub>–NH<sub>2</sub>) were characterized by both Raman spectroscopy and XPS for comparison in **Figure 2**.

Figure 2a compares the N1s core-level XPS spectra of SiO<sub>2</sub>–NH<sub>2</sub> and the SiO<sub>2</sub>–NH<sub>2</sub>/PAA composite film. The two characteristic peaks corresponding to free amine (–NH<sub>2</sub>, 399.6 eV) and hydrogen bonded amine (401.8 eV) were observed in SiO<sub>2</sub>–NH<sub>2</sub>.<sup>[27]</sup> After blending with PAA, the free amine peak at 399.6 eV was greatly reduced. The predominating peak at 401.9 eV is attributed to protonated amine (ammonium, –NH<sub>3</sub><sup>+</sup>) and hydrogen bonded amine, suggesting the formation of the cationic species of the ionic bonds.

The formation of the anionic species (carboxylate, –COO<sup>-</sup>) was confirmed by Raman spectroscopy, as shown in Figure 2b. Characteristic Raman peaks of PAA (indicated by the black dashed lines) were observed at 1690, 1457, 850 cm<sup>-1</sup>, and are attributed to C=O stretching, CH<sub>2</sub> deformation, and C–COOH stretching, respectively.<sup>[28]</sup> When PAA was partially neutralized (80% degree of neutralization, Figure 2b(ii)), new peaks (indicated by the red dashed lines) appeared at 1710, 1417, 903 cm<sup>-1</sup> (C=O stretching, CH<sub>2</sub> deformation, and C–COONa stretching, respectively) due to the formation of carboxylate.<sup>[29]</sup> These three new peaks were present in the spectrum of SiO<sub>2</sub>–NH<sub>2</sub>/PAA, but not in the spectrum of SiO<sub>2</sub>/PAA, confirming the existence of carboxylate in SiO<sub>2</sub>–NH<sub>2</sub>/PAA.

### 2.2. Cycling Performance of Si Composite Anodes

The Si composite anodes were assembled into coin cells with Li counter electrodes to evaluate their electrochemical performance. The anode composition was 60 wt% Si particles, 20 wt% polymer binder, and 20 wt% conductive filler particles. Both PAA and CMC binders were investigated. The battery additive fluoroethylene carbonate (FEC) was added at 10 wt% into battery electrolyte (1 M LiPF<sub>6</sub> in ethylene carbonate/dimethyl carbonate (EC/DMC), 1:1 by volume) to promote the



**Figure 2.** Chemical characterization of functionalized SiO<sub>2</sub> particles and SiO<sub>2</sub> composite films. a) XPS core-level N1s spectra of (i) SiO<sub>2</sub>-NH<sub>2</sub> and (ii) SiO<sub>2</sub>-NH<sub>2</sub>/PAA composite film. Black, purple, and green lines represent raw spectra, smoothed spectra, and baseline, respectively. Blue lines represent deconvoluted N1s of amine groups. Red lines represent deconvoluted N1s of hydrogen bonded nitrogen and ammonium. b) Raman spectra of (i) PAA film, (ii) partially neutralized PAA (80% degree of neutralization) film, (iii) SiO<sub>2</sub>/PAA composite film, and (iv) SiO<sub>2</sub>-NH<sub>2</sub>/PAA composite film.

formation of stable SEI layer on Si particles.<sup>[30–32]</sup> The charge/discharge process was performed between 1 and 0.01 V versus Li/Li<sup>+</sup>. **Figure 3a** shows the voltage profile of different Si composite anodes during the initial charge/discharge cycle at a current density of 0.175 A g<sup>-1</sup>. For all the anodes, the majority of lithiation occurred from 0.1 to 0.01 V and the majority of delithiation occurred from 0.25 to 1 V, consistent with the previous reports for Si composite anodes.<sup>[10]</sup> The specific discharge capacity for the first cycle for all anodes ranged from 2300 to 2700 mAh g<sup>-1</sup>. The initial Coulombic efficiency (ICE, charge capacity/discharge capacity × 100%) for Si anodes with ionic bonding (Si-NH<sub>2</sub>/PAA) was 75%. For electrodes containing CMC and PAA binders with plain Si nanoparticles, only hydrogen bonding is possible between the binder and particles and ICE values were 76% for CMC and 70% for PAA anodes. The irreversible capacity loss from SEI formation (the decomposition of electrolyte on Si particle surfaces) primarily occurs during the first cycle. As a control experiment, Si nanoparticles functionalized with surface methyl groups were used with PAA binder. For this anode composition, no ionic or hydrogen bonding is possible, rather only weak van der Waals interactions between Si-CH<sub>3</sub> and PAA are possible, resulting in a weakly bonded electrode which lowered the ICE to 58%.

The cycling stability and Coulombic efficiency of the Si composite anodes are summarized in **Figure 3b**. Anodes of conventional CMC and PAA binders with no ionic bonding exhibited a significant capacity decrease of ≈65% after 400 cycles. For the Si-CH<sub>3</sub>/PAA control anode, an even faster capacity fade of ≈95% occurred due to the weak bonding of Si-CH<sub>3</sub> with PAA binder. In great contrast, the Si-NH<sub>2</sub>/PAA anode with ionic bonding exhibited excellent cycling stability. The discharge

capacity after 400 cycles was 1177 mAh g<sup>-1</sup> corresponding to 80% capacity retention. These results suggest that the ionic bonding is more effective than hydrogen bonding in preserving the integrity of the electrode and repairing the damage in the conductive network caused by the volume change during cycling. An increase of capacity was consistently observed for Si-NH<sub>2</sub>/PAA, Si/PAA, and Si/CMC anodes during the initial (0–50) cycles (**Figure 3b**). Though similar results have been reported previously, the origin of this increase is not well understood.<sup>[11,33]</sup> An increase in capacity is possibly due to increased wetting of the electrolyte into the composite anode during cycling.

The morphology change of Si-NH<sub>2</sub>/PAA anodes after cycling was examined by Scanning Electron Microscopy (SEM), as shown in **Figure 4** (cross-sectional images). Prior to cycling, discrete Si particles and carbon black particles were observed in the composite anode with uniform distribution. Upon cycling, the anode surface became smooth due to the formation of SEI layer on the surface of both Si and carbon black particles. The volume expansion (percentage thickness increase of electrodes) upon 400

cycles for both Si-NH<sub>2</sub>/PAA and Si/PAA was estimated from cross-sectional SEM images as ≈80% (**Figure S1** and **Table S1**, Supporting Information). The composition of the SEI layer was further studied by XPS and the results are summarized in **Figure 5**. The N1s core-level XPS spectra of pristine and cycled anodes are shown in **Figure 5a**. The formation of ionic bonds was confirmed by the presence of protonated amine (-NH<sub>3</sub><sup>+</sup>) in the pristine anode. After 400 cycles, no N1s signal was detected, suggesting the formation of an SEI layer on the Si particle surface. Similarly, the C1s signals from carbon black and PAA disappeared after cycling (**Figure 5b**), further demonstrating the formation of SEI layers on carbon black surface and on PAA binder.

To further explore the effect of ionic bonding on cycling performance, we tested Si composite anodes with different concentrations of ionic bonding. The XPS characterization revealed that all the amino groups were converted to ammonium ions in the composite anode. Hence, the concentration of ionic bonding in the anodes was controlled by the amine coverage on the Si particle surface. **Figure 6** shows the cycling stability of Si composite anodes made with Si nanoparticles with different amine coverages. Initially, all of the anodes had similar discharge capacity peaking of ≈1500 mAh g<sup>-1</sup> at about 50 cycles. The as-received Si (no amine functional groups) anode lost 70% of its capacity after 400 cycles. Significant improvement on anode capacity retention was observed when amine functionalized Si was used and the amine coverage increased from 0.016 mmol g<sup>-1</sup> Si to 0.050 mmol g<sup>-1</sup>. The increased capacity retention of Si composite anodes is clearly correlated with an increase in amine coverage on Si particles and the resultant increase in ionic bonding concentration in the Si anodes.

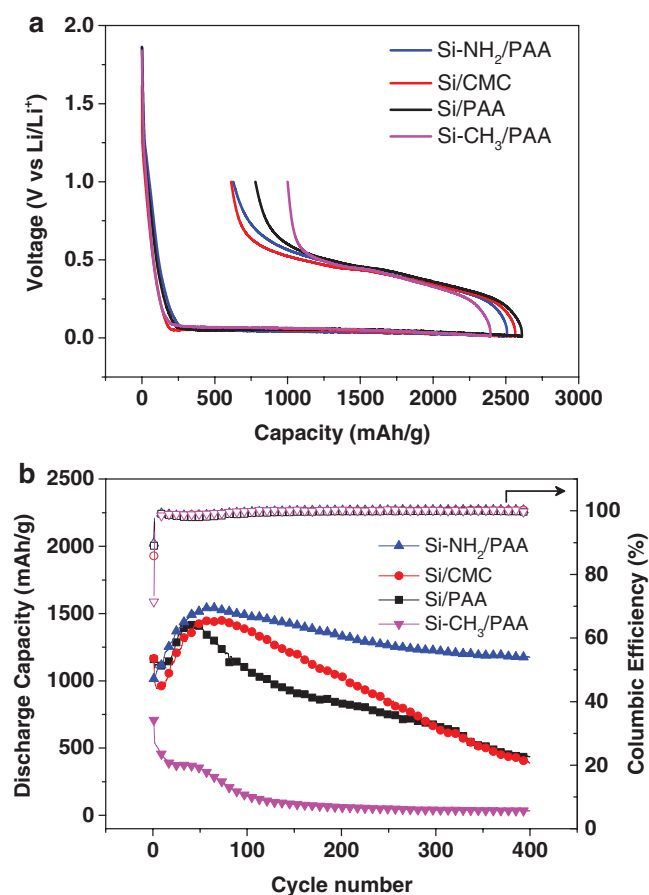


**Figure 3.** Cycling performance of Si composite electrodes. a) Initial voltage–capacity profile of Si composite anodes at a current density of  $0.175 \text{ A g}^{-1}$  between 0.01 and 1.0 V versus  $\text{Li/Li}^+$ . b) Discharge capacity (solid symbols) and Coulombic efficiency (open symbols) of Si composite anodes at a current density of  $2.1 \text{ A g}^{-1}$  between 0.01 and 1.0 V versus  $\text{Li/Li}^+$ . The anodes were preconditioned with a single formation cycle at a current density of  $0.175 \text{ A g}^{-1}$  (results not shown). All cycling experiments used  $1 \text{ M LiPF}_6 \text{ EC/DMC}$  (1:1 by volume) electrolyte with 10 wt% FEC additive. The capacity was normalized by the weight of Si particles.

The electrochemical performance of Si composite anodes with ionic bonding was also evaluated at different cycling rates. **Figure 7** shows the capacity and Coulombic efficiency with respect to different cycling rates. The current density was increased from  $0.21 \text{ A g}^{-1}$  ( $C/20$ ) to  $4.2 \text{ A g}^{-1}$  ( $1C$ ) at five different

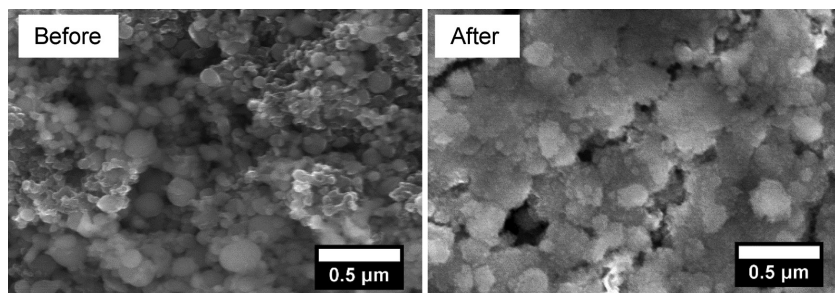


**Figure 4.** Cross-sectional SEM images of  $\text{Si-NH}_2/\text{PAA}$  composite anode before and after cycling. The anode was cycled at a current density of  $2.1 \text{ A g}^{-1}$  between 0.01 and 1.0 V versus  $\text{Li/Li}^+$  for 400 cycles.

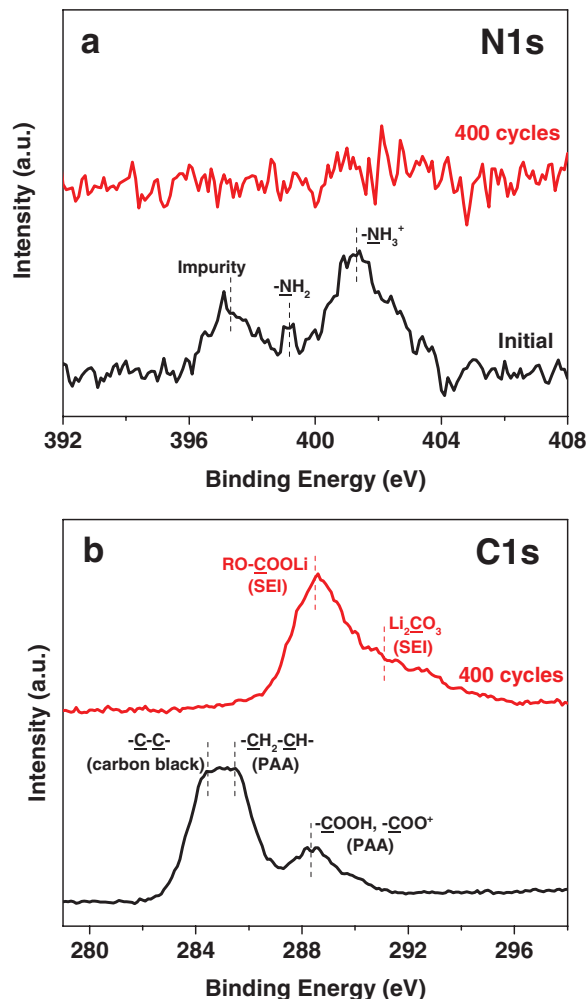


**Figure 5.** XPS spectra of  $\text{Si-NH}_2/\text{PAA}$  anode surface before (black curves) and after 400 cycles (red curves). a)  $\text{N1s}$ , b)  $\text{C1s}$ . The anode was cycled at a current density of  $2.1 \text{ A g}^{-1}$  between 0.01 and 1.0 V versus  $\text{Li/Li}^+$ .

cycling rates, and then reduced back to  $0.21 \text{ A g}^{-1}$ . After the initial ten cycles at  $0.21 \text{ A g}^{-1}$ , the reversible capacity remained above  $2000 \text{ mAh g}^{-1}$ . The initial gradual increase of capacity is consistent with the cycling results in **Figures 3b** and **6**. As expected, a decrease of capacity was observed with increasing current density.<sup>[34]</sup> At the highest current density of  $4.2 \text{ A g}^{-1}$ , the anode still retained a high capacity of  $\approx 1150 \text{ mAh g}^{-1}$ .

When the current density was brought back to  $0.21 \text{ A g}^{-1}$ , the capacity was fully recovered to  $\approx 2100 \text{ mAh g}^{-1}$ , suggesting no permanent damage of anode during the entire cycling test.

The resistance change of the Si composite anodes with ionic bonding was characterized by electrochemical impedance spectroscopy. The measurements were performed at the fully delithiated state of the anodes by holding the voltage at 1 V versus  $\text{Li/Li}^+$  for 6 h after a specific charging cycle. The Nyquist plots of the  $\text{Si-NH}_2/\text{PAA}$  anodes are shown in **Figure 8a**. The response resembles

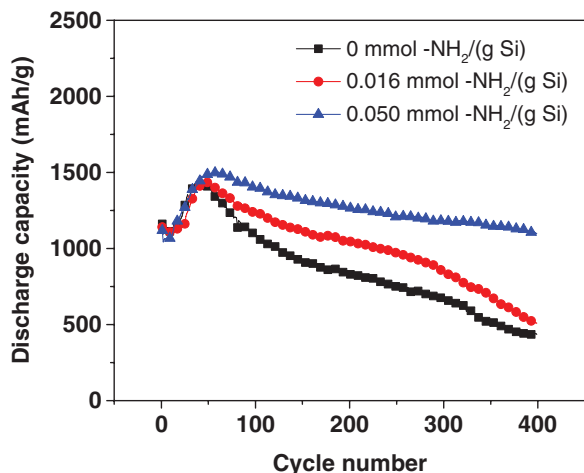


**Figure 6.** Electrochemical cycling performance of Si composite anodes with different amine coverages on Si particles. The anodes were cycled at a current density of  $2.1 \text{ A g}^{-1}$  between 0.01 and 1.0 V versus Li/Li<sup>+</sup>. The anodes were preconditioned with a single formation cycle at a current density of  $0.175 \text{ A g}^{-1}$  (results not shown). The capacity was normalized by the weight of Si particles.

a semicircle in the high-frequency range followed by a line in the low-frequency range within each plot. The change of charge transfer resistance and SEI resistance was obtained by fitting the Nyquist plot to an equivalent circuit model in the 200 kHz–1 Hz region (see the Supporting Information).<sup>[35]</sup> As shown in **Figure 9**, both the charge transfer resistance and SEI resistance of the Si-NH<sub>2</sub>/PAA anode remained the same throughout the test, indicating that the anode maintained a robust conductive network with a stable SEI. Moreover, the stable charge transfer resistance over 300 cycles correlates with the superior capacity retention (Figure 3b) of our Si composite anodes. In comparison, Si composite anodes (Si/PAA) without ionic bonding showed comparable charge transfer resistance and SEI resistance values as those of Si-NH<sub>2</sub>/PAA anodes at the first few cycles, but then showed a steady and significant increase in

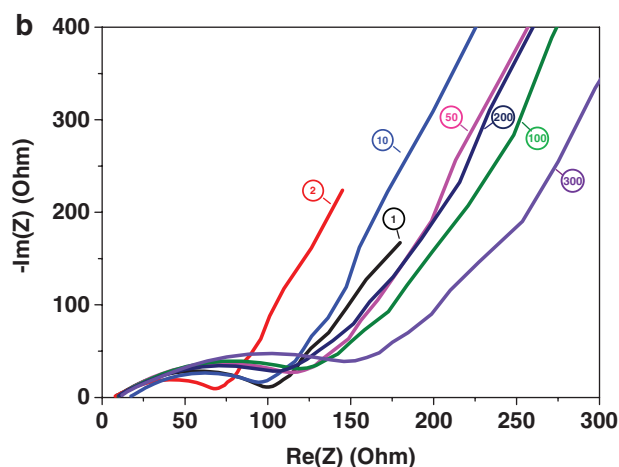
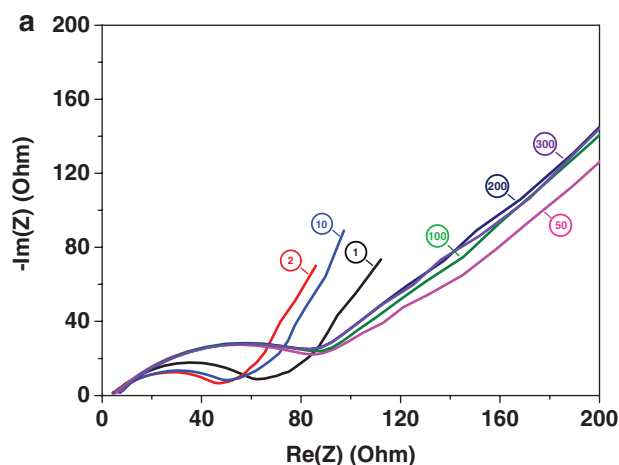


**Figure 8.** Impedance testing results for a) Si-NH<sub>2</sub>/PAA and b) Si/PAA composite anode. The anodes were cycled at a current density of  $2.1 \text{ A g}^{-1}$  between 0.01 and 1.0 V versus Li/Li<sup>+</sup>. The circled number refers to the cycle number of galvanostatic cycling and impedance was measured after completion of the entire discharge/charge cycle. Si nanoparticles in Si-NH<sub>2</sub>/PAA anode have amine coverage of  $0.050 \text{ mmol g}^{-1}$  Si.

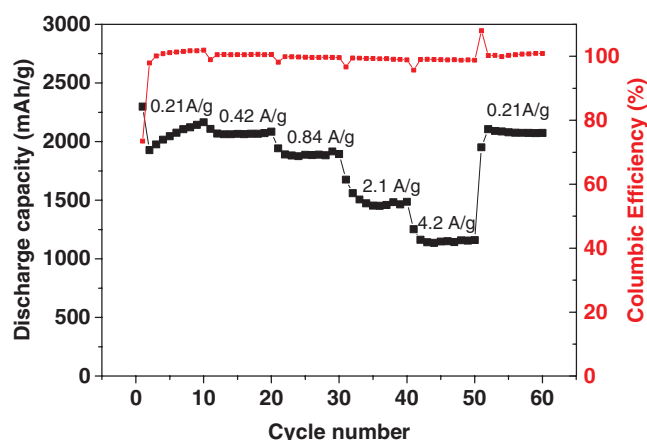


**Figure 7.** Discharge capacity and Coulombic efficiency of Si-NH<sub>2</sub>/PAA composite anode at various current densities cycled between 0.01 and 1.0 V versus Li/Li<sup>+</sup>. The capacity was normalized by the weight of Si particles. Si nanoparticles in this study have amine coverage of  $0.050 \text{ mmol g}^{-1}$  Si.

both resistances (Figures 8b and 9), agreeing with the observation of decreased capacity over 300 cycles (Figure 3b).

### 3. Conclusion

A novel dynamic bonding scheme was developed to increase the cycle lifetimes and reliability of Si composite anodes. Si composite anodes with increased capacity retention were achieved through dynamic ionic bonding at the interface between Si nanoparticles and a polymeric PAA binder. Amine groups were covalently attached to the surface of Si nanoparticles. During anode fabrication, ionic bonds were readily formed between the amine groups on Si particle surfaces and the carboxyl groups on the PAA binder and confirmed by X-ray photoelectron and Raman spectroscopy. The dynamic ionic bonds effectively mitigated the degradation in capacity that occurs due to the large volume change of Si anodes during lithium intercalation. We demonstrated Si composite anodes with capacity retention

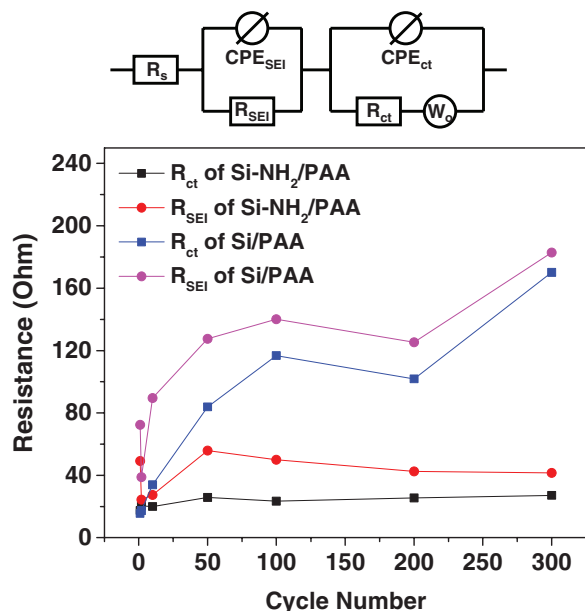


**Figure 9.** Change of SEI resistance ( $R_{SEI}$ ) and charge transfer resistance ( $R_{ct}$ ) for Si-NH<sub>2</sub>/PAA and Si/PAA composite anodes over 300 cycles at a current density of 2.1 A g<sup>-1</sup> between 0.01 and 1.0 V versus Li/Li<sup>+</sup>.  $R_{SEI}$  and  $R_{ct}$  were calculated by fitting the Nyquist plots (200 kHz–1 Hz data) with the corresponding equivalent circuit.  $R_s$ , cell internal Ohmic resistance;  $R_{SEI}$ , the resistance from SEI layer;  $R_{ct}$ , the resistance from charge transfer reaction; Constant Phase Element, CPE<sub>SEI</sub>, the capacitance of the SEI layer; CPE<sub>ct</sub>, the capacitance of double layer; and  $W_o$ , Warburg element describing the solid state Li ion diffusion process. Si nanoparticles in Si-NH<sub>2</sub>/PAA anode have amine coverage of 0.050 mmol g<sup>-1</sup> Si.

of ≈80% for 400 cycles at a current density of 2.1 A g<sup>-1</sup> (C/2). The Si composite anodes with ionic bonding also demonstrated good rate capability with retention of high capacity (1150 mAh g<sup>-1</sup>) at 4.2 A g<sup>-1</sup> (1C).

#### 4. Experimental Section

**Materials:** Trimethoxymethylsilane, APS, sodium CMC (average  $M_w \approx 700\,000$ ), PAA (average  $M_w \approx 1\,250\,000$ ), ninhydrin, and sodium hydroxide were used as received from Sigma-Aldrich. Silicon nanoparticles (99%, 100 nm, plasma synthesized) were purchased from MTI Corporation. Battery electrolyte containing 1 M lithium hexafluorophosphate (LiPF<sub>6</sub>) in a mixture of EC and DMC (1:1 by volume) was purchased from BASF. Carbon black (Regal 400R) was obtained from Cabot Corporation. FEC and lithium metal (0.75 mm in thickness) were purchased from Alfa Aesar. The battery separator film was a trilayer polypropylene–polyethylene–polypropylene membrane made by Celgard and was purchased from MTI Corporation.

**Surface functionalization of Si particles and amine coverage:** The Si nanoparticles (1.0 g) were dispersed in ethanol (60 mL). An appropriate amount of APS was then added into the stirring suspension. After 2 d, the amine functionalized Si particles were centrifuged, rinsed with ethanol for three times, and vacuum dried. Silica nanoparticles were also functionalized with amine following the same procedure for Raman and XPS characterization. Trimethoxymethyl silane was used to make methyl functionalized Si particles for control samples.

The coverage of amino groups on the surface of Si nanoparticles was characterized by a ninhydrin titration method.<sup>[36]</sup> Ninhydrin is known to react with primary amine to produce a purple color complex. The concentration of the complex (equal to the concentration of amino

groups) is determined by measuring the UV–vis absorbance (@588 nm) of the reaction solution. The amine functionalized Si (0.02 g) was dispersed in ethanol (2.8 mL) and sonicated for 20 min. A ninhydrin solution (0.35 w/v% ninhydrin in ethanol, 1.0 mL) was then added to the suspension. After 10 min of sonication, the mixture was heated at 80 °C for 20 min. Upon cooling down, the mixture was centrifuged and the supernatant was collected for UV–vis (UV-2401 PC, Shimadzu, Japan) measurement. A linear calibration curve was created by measuring the UV–vis absorbance (@588 nm) of a reaction solution of hexylmethylenediamine and ninhydrin with five known concentrations. The concentration of amino groups on Si–NH<sub>2</sub> was determined from the calibration curve.

**Preparation of Si composite anodes and structural characterization of ionic bonds:** Si composite anodes were prepared with a weight ratio of 60:20:20 of Si nanoparticles, polymer binder, and carbon black. Two different binders were investigated: PAA and CMC. The binder (30 mg) was dissolved in deionized (DI) water (3 g), and then Si (90 mg) and carbon black (30 mg) particles were added to the solution subsequently. The pK<sub>a</sub> of PAA was around 4.2, the pH of the Si–NH<sub>2</sub>/PAA slurry (0.3 wt% Si–NH<sub>2</sub> and 0.1% PAA in DI water) was 3.75 and the pH of the PAA alone (0.1 wt% PAA in DI water, no Si–NH<sub>2</sub>) was 3.70. Any significant change in pH with the addition of Si–NH<sub>2</sub> was not measured. The mixture was homogenized (OMNI GLH-01) for 1 h and magnetically stirred for 2 d. The slurry was cast on Cu foil (thickness ≈8 μm) with a doctor blade and air dried. After drying, the gravimetric loading was ≈0.5–0.8 mg cm<sup>-2</sup> (total electrode mass) and theoretical areal capacity loading was 1.2–2.0 mAh cm<sup>-2</sup> (based on 4200 mAh g<sup>-1</sup> theoretical capacity for Si).

XPS (Kratos Axis ULTRA) and Raman spectroscopy (Horiba LabRAM HR 3D) were used to characterize ionic bond formation in Si anodes. Films with different compositions were made by casting the particle or particle/polymer suspensions onto plastic substrate followed by air drying.

**Electrochemical characterization of Si anodes:** The Si anodes were dried at 80 °C in argon atmosphere for 8 h and assembled into 2032 type stainless steel coin cells with Li metal as the counter electrode in an Ar-filled glove box. The electrolyte used was 1 M LiPF<sub>6</sub> in EC/DMC with 10 wt% FEC.

The cells were electrochemically cycled between 0.01 and 1.0 V versus Li/Li<sup>+</sup> at C/24 rate for the first formation cycle with first discharge step starting from open circuit voltage (≈2 V vs Li/Li<sup>+</sup>) and different rates for the subsequent cycles using a battery test station (Arbin BT2000). For C/24 rate, the current density was 0.175 A g<sup>-1</sup> (normalized by Si only) or ≈0.05–0.08 mA cm<sup>-2</sup>. For C/2 rate, the current density was 2.1 A g<sup>-1</sup> (normalized by Si only) or ≈0.6–1.0 mA cm<sup>-2</sup>. Impedance was measured on a potentiostat system (Bio-Logic VSP) with a frequency range of 200 kHz–0.1 Hz at 1 V with 10 mV amplitude. The cells were discharged at 1 V for 6 h prior to impedance measurement.

**Characterization of Si Anodes:** SEM (Hitachi 4800) and XPS were used to characterize the morphological and structural change of Si composite anodes upon cycling. The cycled coin cell was disassembled in an Ar filled glove box. The cycled anode was rinsed with DMC three times to remove residual electrolyte and dried in an argon atmosphere prior to SEM and XPS characterization.

#### Supporting Information

Supporting Information is available from the Wiley Online Library or from the author.

#### Acknowledgements

This work was supported as part of the Center for Electrochemical Energy Science, an Energy Frontier Research Center funded by the U.S. Department of Energy, Office of Science, Basic Energy Sciences.

## Conflict of Interest

The authors declare no conflict of interest.

## Keywords

ionic bonding, Li-ion batteries, restoration of electrical interfaces, Si composite anodes

Received: January 5, 2017

Revised: March 10, 2017

Published online:

- 
- [1] M. Armand, J. M. Tarascon, *Nature* **2008**, 451, 652.  
 [2] J. M. Tarascon, M. Armand, *Nature* **2001**, 414, 359.  
 [3] H. Wu, Y. Cui, *Nano Today* **2012**, 7, 414.  
 [4] X. Su, Q. Wu, J. Li, X. Xiao, A. Lott, W. Lu, B. W. Sheldon, J. Wu, *Adv. Energy Mater.* **2014**, 4, 1300882.  
 [5] F. Luo, B. Liu, J. Zheng, G. Chu, K. Zhong, H. Li, X. Huang, L. Chen, *J. Electrochem. Soc.* **2015**, 162, A2509.  
 [6] M. Ashuri, Q. He, L. L. Shaw, *Nanoscale* **2016**, 8, 74.  
 [7] U. Kasavajjula, C. Wang, A. J. Appleby, *J. Power Sources* **2007**, 163, 1003.  
 [8] X. Li, M. Gu, S. Hu, R. Kennard, P. Yan, X. Chen, C. Wang, M. J. Sailor, J.-G. Zhang, J. Liu, *Nat. Commun.* **2014**, 5, 4105.  
 [9] Z. Zhang, Y. Wang, W. Ren, Q. Tan, Y. Chen, H. Li, Z. Zhong, F. Su, *Angew. Chem., Int. Ed. Engl.* **2014**, 126, 5265.  
 [10] B. Koo, H. Kim, Y. Cho, K. T. Lee, N. S. Choi, J. Cho, *Angew. Chem., Int. Ed. Engl.* **2012**, 51, 8762.  
 [11] M. H. Ryou, J. Kim, I. Lee, S. Kim, Y. K. Jeong, S. Hong, J. H. Ryu, T. S. Kim, J. K. Park, H. Lee, J. W. Choi, *Adv. Mater.* **2013**, 25, 1571.  
 [12] I. Kovalenko, B. Zdyrko, A. Magasinski, B. Hertzberg, Z. Milicev, R. Burtovyy, I. Luzinov, G. Yushin, *Science* **2011**, 334, 75.  
 [13] J. Li, R. B. Lewis, J. R. Dahn, *Electrochem. Solid-State Lett.* **2007**, 10, A17.  
 [14] Z. J. Han, N. Yabuuchi, K. Shimomura, M. Murase, H. Yui, S. Komaba, *Energy Environ. Sci.* **2012**, 5, 9014.  
 [15] J. S. Bridel, T. Azaïs, M. Morcrette, J. M. Tarascon, D. Larcher, *Chem. Mater.* **2009**, 22, 1229.  
 [16] C. Wang, H. Wu, Z. Chen, M. T. McDowell, Y. Cui, Z. Bao, *Nat. Chem.* **2013**, 5, 1042.  
 [17] J. Lopez, Z. Chen, C. Wang, S. C. Andrews, Y. Cui, Z. Bao, *ACS Appl. Mater. Interfaces* **2016**, 8, 2318.  
 [18] Y. Sun, J. Lopez, H.-W. Lee, N. Liu, G. Zheng, C.-L. Wu, J. Sun, W. Liu, J. W. Chung, Z. Bao, Y. Cui, *Adv. Mater.* **2016**, 28, 2455.  
 [19] R. J. Wojtecki, M. A. Meador, S. J. Rowan, *Nat. Mater.* **2011**, 10, 14.  
 [20] K. Xu, *Chem. Rev.* **2004**, 104, 4303.  
 [21] J. Y. Sun, X. Zhao, W. R. K. Illeperuma, O. Chaudhuri, K. H. Oh, D. J. Mooney, J. J. Vlassak, Z. Suo, *Nature* **2012**, 489, 133.  
 [22] Z. Wei, J. He, T. Liang, H. Oh, J. Athas, Z. Tong, C. Wang, Z. Nie, *Polym. Chem.* **2013**, 4, 4601.  
 [23] D. V. Andreeva, D. Fix, H. Möhwald, D. G. Shchukin, *Adv. Mater.* **2008**, 20, 2789.  
 [24] A. B. South, L. A. Lyon, *Angew. Chem., Int. Ed. Engl.* **2010**, 49, 767.  
 [25] T. Bayer, K. J. Eichhorn, K. Grundke, H. J. Jacobasch, *Macromol. Chem. Phys.* **1999**, 200, 852.  
 [26] X. Song, J. Zhai, Y. Wang, L. Jiang, *J. Colloid Interface Sci.* **2006**, 298, 267.  
 [27] B. Lindberg, R. Maripuu, K. Siegbahn, R. Larsson, C. G. Gölander, J. C. Eriksson, *J. Colloid Interface Sci.* **1983**, 95, 308.  
 [28] J. Dong, Y. Ozaki, K. Nakashima, *J. Polym. Sci., Part B: Polym. Phys.* **1997**, 35, 507.  
 [29] S. Koda, H. Nomura, M. Nagasawa, *Biophys. Chem.* **1983**, 18, 361.  
 [30] J. Song, M. Zhou, R. Yi, T. Xu, M. L. Gordin, D. Tang, Z. Yu, M. Regula, D. Wang, *Adv. Funct. Mater.* **2014**, 24, 5904.  
 [31] H. Nakai, T. Kubota, A. Kita, A. Kawashima, *J. Electrochem. Soc.* **2011**, 158, A798.  
 [32] Y.-M. Lin, K. C. Klavetter, P. R. Abel, N. C. Davy, J. L. Snider, A. Heller, C. B. Mullins, *Chem. Commun.* **2012**, 48, 7268.  
 [33] H. Wu, G. Yu, L. Pan, N. Liu, M. T. McDowell, Z. Bao, Y. Cui, *Nat. Commun.* **2013**, 4, 1943.  
 [34] C. K. Chan, H. Peng, G. Liu, K. McIlwrath, X. F. Zhang, R. A. Huggins, Y. Cui, *Nat. Nanotechnol.* **2008**, 3, 31.  
 [35] B. Li, F. Yao, J. J. Bae, J. Chang, M. R. Zamfir, D. T. Le, D. T. Pham, H. Yue, Y. H. Lee, *Sci. Rep.* **2015**, 5, 7659.  
 [36] E. Soto-Cantu, R. Cueto, J. Koch, P. S. Russo, *Langmuir* **2012**, 28, 5562.